ISSN PRINT 2319 1775 Online 2320 7876
 UGC CARE Listed (Group -I) Journal Volume 12, Iss 01, 2023

THICKNESS EFFECTS ON THE PHYSICAL CHARACTERIZATION OF NANOSTRUCTURED CUO THIN FILMS

Anil Kumar Bedwal, Vikram Singh*

Research Scholar, OM Sterling Global University, Hisar, Email id:

Assistant Professor, OM Sterling Global University, Hisar, Email id:
Anilkumarbedwal9@gmail.com, Vikramdobal@gmail.com

Corresponding Author: Vikram Singh

Abstract:

Nanostructured CuO thin films on glass substrates of varying thicknesses (250, 300, and 350 nm) were produced in these investigations using radio frequency (RF) magnetron sputtering. The films' X-ray diffraction (XRD) results showed a polycrystalline structure, with the (111) plane being the most prominent peak. Grain size was calculated using the Scherrer formula. As the film thickness increases from 250 nm to 3000 nm and then 300 nm, the average grain sizes decrease and reach 10.78 nm, 11.36 nm, and 11.84 nm, respectively. Nucleus scan microscopy (AFM) results showed that surface roughness dropped from 9.30 nm to 4.71 nm with increasing thickness. The root mean square (RMS) roughness also dropped from 9.18 nm to 4.29 nm as the layer thickness increased. Scanning electron microscopy (SEM) pictures show that the particles in the homogeneous, semi-spherical structure are evenly dispersed.

Keywords: CuO, sensing, Thickness, Structural, Morphological

INTRODUCTION

Since energy supplies are essential for both business and home usage, energy is an important concern. As the global economy continues to grow at an unprecedented pace, two major concerns have emerged about the future of our energy supply: first, the eventual exhaustion of conventional fossil fuels, and second, the escalation of pollution and greenhouse gas emissions. Therefore, it is of the utmost importance to create and sell renewable energy sources that are safe for the environment, as well as the technology that backs them up. The combustion of fossil fuels, the primary source of energy, has the potential to significantly alter global ecosystems and economies. Consequently, there was a significant need for renewable energy storage solutions that are cost-effective, very efficient, and kind to the environment.

A simple and cheap hydrothermal synthesis method was used to create nanostructured CuO thin films using copper sulfate (CuSO4). Here, we study the effects of CuSO4 concentration on supercapacitor performance, crystallinity, and morphology. A supercapacitor relies on an electrolyte solution. Electrolytes with higher ionic conductivity and sufficient ion supply may enhance capacitance by intercalating into host oxides, which can subsequently store the ions in their bulk. Here, the electrolyte is an ionic liquid known as [HPMIM][Cl]. To create nano-structured cuO material, a new ionic liquid electrolyte made of (HPMIM)(Cl) is used, and the

preparative conditions are adjusted. Cyclic voltammetry, electrochemical impedance, scanning electron microscopy, X-ray diffraction, and galvanostatic charge-discharge In order to examine the CuO nanostructure, spectroscopy was used. The specific capacitance of the electrode is computed.

Copper oxide (CuO) has a lot of potential as an electrode material for supercapacitors since it is cheap, has strong pseudocapacitve qualities, and doesn't harm the environment. Comparatively, CuO outperforms other metal oxides, such as MnO2, NiO, and CoO, due to its chemical stability and the ease with which it can be fabricated at the nanoscale in a number of different forms. However, many things remain unclear, and it has not yet reached its maximum potential. There is little information available on the usage of thin films of CuO in pseudo supercapacitors. Electrode materials: the concept and implementation of copper oxide (CuO). They successfully synthesized cauliflower-, nanobelt-, and feather-like CuO nanostructures using a straightforward chemical bath deposition system. A longer length of discharge was seen with the cauliflower-like shape. Altering the geometry of CuO transport might improve the material's temporal electrochemical properties, according to their study. Electrons and, subsequently, electrolytic ions, are able to diffuse more easily through CuO's cauliflower structure. Thin amorphous and porous CuO films were electrodeposited; their specific capacitance is 36Fg-1. Chemical bath deposition from hierarchical multilayer nano-sheet clusters was used to generate thin films of CuO. Approximate specific capacitance is 43 Fg−1. The low specific capacitance value is believed to be caused by films with lower electronic conductivity and neutral electrolytes with limited ionic conductivity. One reason neutral electrolytes are utilized is because CuO is unstable in acidic conditions.

Some semiconductors, such photovoltaic cells, antibacterial activities, sensing, magnetic storage media, and supercapacitors, are either used extensively or are being investigated for potential uses in many different sectors. Band gaps in nanostructured CuO range from 1.4 to 3.1 eV. One possible use for materials such as CuO and Cu2O is in the production of junction devices such as pn junction diodes, as they are often thought of as p-type semiconductors. Cupric oxide is abundant and safe to use because of its components. Because of these advantages, their use in other industries, such as photovoltaic devices and power sources, has garnered a lot of attention. The deposition of nanostructured CuO films may be accomplished by a variety of techniques, including chemical vapor deposition (CVD), electrodeposition technique, reflux condensation, SILAR, sol-gel spin-coating procedure, spray pyrolysis, thermal oxidation, and magnetron sputtering. Using XRD, AFM, and UV-VIS spectroscopy, this study synthesized nanostructured copper oxide films of varying thicknesses using RF magnetron sputtering.

MATERIAL AND METHODS

Materials:

- **Target Material**: 99.99% pure CuO.
- **Substrate**: Glass substrates were used to deposit the thin films.

Methods:

1. **Deposition Method**:

- **Technique**: The thin films were deposited using Radio Frequency (RF) magnetron sputtering.

- **Pre-sputtering**: The oxide layer was pre-sputtered in an argon atmosphere.

- **Sputtering Chamber**: The chamber was evacuated to a pressure of 5×10−55 \times 10^{-5}5×10−5 mbar using a turbomolecular pump.

- **Film Thickness**: Films were deposited with thicknesses of 250 nm, 300 nm, and 350 nm.

2. **Characterization Techniques**:

- **X-Ray Diffraction (XRD)**: Used to study the crystallographic properties of the CuO films and calculate the grain size using Scherrer's formula.

- **Atomic Force Microscopy (AFM)**: Analyzed the surface morphology and measured surface roughness.

- **Scanning Electron Microscopy (SEM)**: Used to investigate the surface morphology and particle distribution of the thin films.

- **Spectrophotometry**: Optical analysis for transmission data in the range of 300-900 nm.

3. **Gas Sensor Testing**:

- A specific gas sensor testing setup was used, as shown in Figure 1 of the paper.

4. **Electrochemical Analysis**:

- **Electrochemical Impedance Spectroscopy (EIS)**: Performed using a three-electrode cell setup with a platinum counter electrode and saturated calomel electrode (SCE) as the reference. Graphite served as the counter electrode.

- **Electrolyte**: 0.1M [HPMIM][Cl] ionic liquid was used as the electrolyte.

These methods provide a comprehensive approach to understanding how film thickness influences the structural, morphological, and electrochemical properties of nanostructured CuO thin films

EXPERIMENTAL

A process known as RF magnetron sputtering was used to deposit oxide layers. An oxide layer was removed from a 99.99% pure CuO target by pre-sputtering it in an argon atmosphere before commencing. The sputtering chamber was evacuated to a pressure of 5x10-5 mbar using the turbomolecular pump. The substrate, which was glass, was used to generate thin films. The XRD pattern allows us to study the CuO films' crystallographic properties. Using a weighing technique, the film thickness was determined to be (250, 300, and 350) nm. The crystal structure's behavior was investigated using the XRD technique. By

ISSN PRINT 2319 1775 Online 2320 7876
 UGC CARE Listed (Group -I) Journal Volume 12, Iss 01, 2023

using the tapping mode of the Nanoscope IIIa scanning probe microscope controller, AFM pictures were obtained for morphological studies. A scanning electron microscope (SEM), specifically a Shimadzu 3101 PC, was used to examine the deposited thin film's morphology. For the optical analysis, spectrometer data for the (300 - 900 nm) range of optical transmission were used. The testing method shown in Figure (1) was used to monitor gas levels.

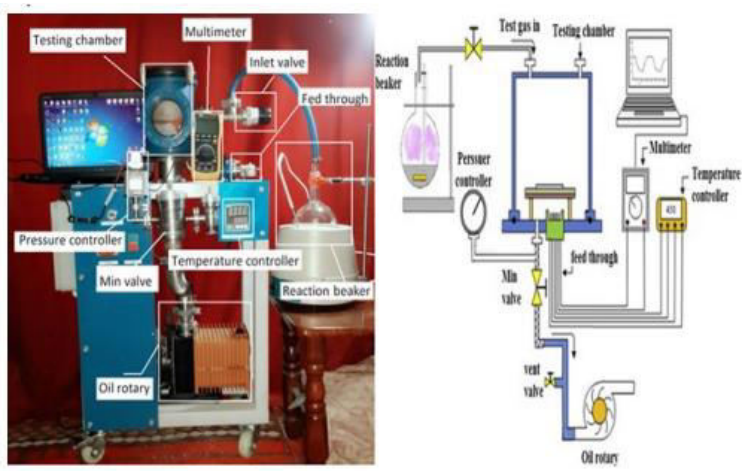

Fig. 1. Gas sensor testing system

Results and discussion

XRD

The X-ray diffraction (XRD) patterns for different film thicknesses (250 nm, 300 nm, and 350 nm) are illustrated in Figure 2. In comparison to the standard JCPDS card No. (05-0661), the analysis revealed that the grown films exhibit a polycrystalline monoclinic structure. This finding aligns with the results reported by Mageshwari et al. [14]. The identified crystallographic planes include (110), (111), (020), and (220), with corresponding peaks observed at (2θ=32.25°, 38.37°, 53.43°, and 65.43°), respectively. These results are in accordance with previous studies [22, 23], confirming the consistency of the observed crystallographic characteristics with established literature in the field. Debye-Scherrer's formula was employed to evaluate crystallite size (D) is given by [24, 25]:

$$D = \frac{0.94\lambda}{\beta cos\theta}$$

where θ is the Bragg angle, β is FWHM, and λ is the wavelength. Since increasing thickness results lead to increase in the grain size, the increase in film thickness could cause these modifications, resulting in an enhancement in film crystallinity, rearranging of atoms, and the elimination of defects [26]. Similar research for thin films with a thickness of 350 nm has been published.

Dislocation density (δ) is calculated from Eq.:

ISSN PRINT 2319 1775 Online 2320 7876
 UGC CARE Listed (Group -I) Journal Volume 12, Iss 01, 2023

$$\delta = \frac{1}{D^2}$$

strain (ε) is calculated from the following Eq.

$$\varepsilon = \frac{\beta cos\theta}{4}$$

According to Table 1, dislocation density and strain reduced as thickness increased. As the thickness increases, the peak locations remain unchanged. Thin CuO films with 250 nm and 350 nm thickness have the same lattice constant and volume cell. This behavior matches well with [18]. Figure (3) displays FWHM, D, δ and ε versus different thicknesses.

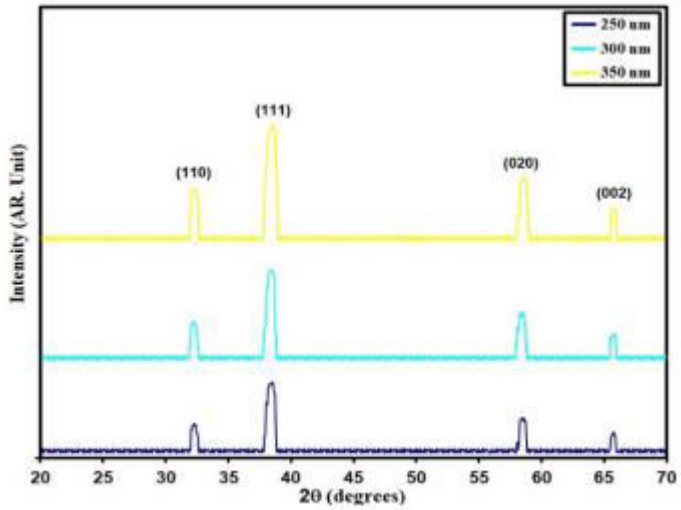

Fig.2. XRD of grown films

Table 1. XRD parameters and energy gap of grown films

Thickness (nm)	2 (°)	(hkl) Plane	FWHM (°)	E_g (eV)	*D* (nm)	δ (× 10^{14}) (lines/m^2)	ε (×10^{-4})
250	38.37	111	0.78	2.54	10.78	85.92	32.13
300	38.35	111	0.74	2.49	11.36	77.36	30.49
350	38.30	111	0.71	2.41	11.84	71.33	29.26

ISSN PRINT 2319 1775 Online 2320 7876
 UGC CARE Listed (Group -I) Journal Volume 12, Iss 01, 2023

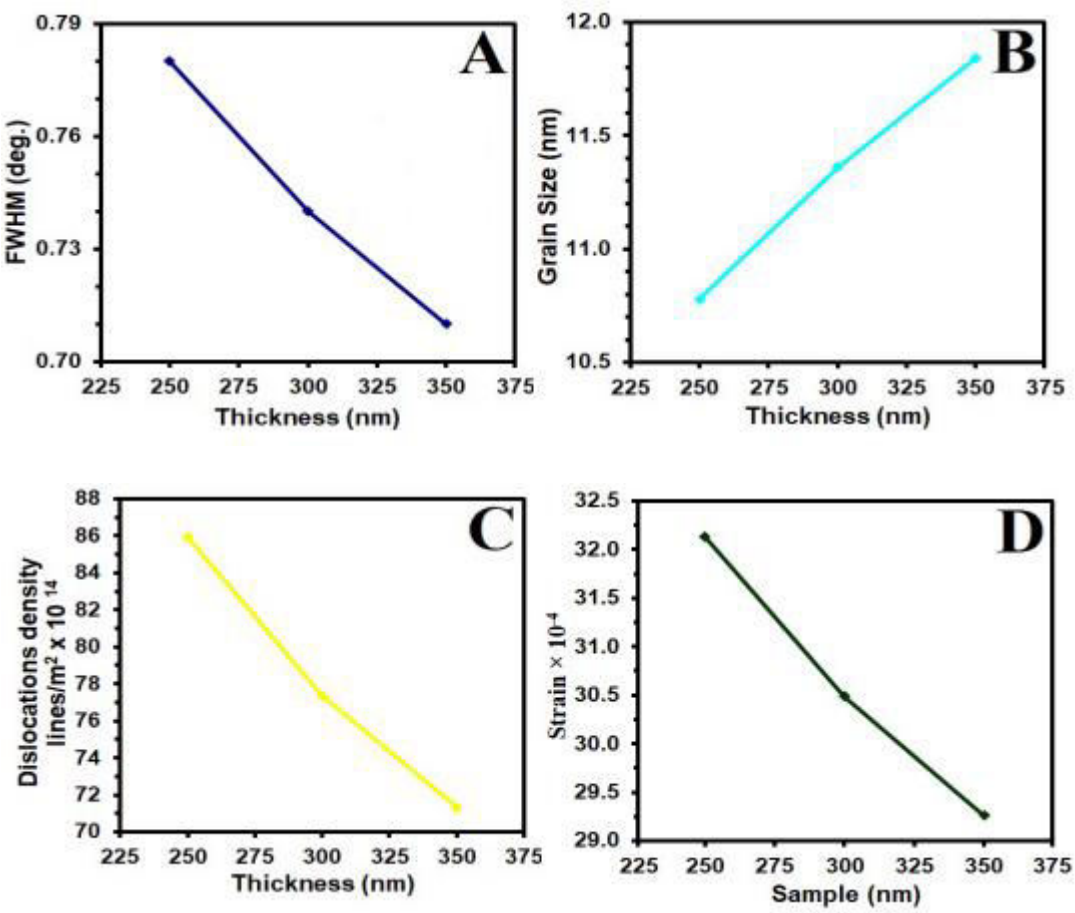

Fig. 3. XRD parameters of CuO films.

Scanning Electron Microscopic Image

Scanning electron microscopy is a powerful tool for nanoscale spatial resolution imaging of materials. During these tests, a focused electron beam captures the surface topography of the conductive sample. Examining the SEM pictures obtained by a scanning electron microscope (JEOL-JSM-6360, Japan) operating at 20kV allowed for the investigation of the films' surface morphology.

To identify the effect of CuSO4 precursor concentration, scanning electron microscopy (SEM) was used to investigate the morphology of the deposited samples. At a magnification of ×5000, all the samples, spanning from CuO0.1M to CuO0.5M, are shown in Fig. 4 (a-e). All of the samples display the microgranular morphology, independent of the precursor solution concentration. These micro-grains are topped by nano-petal-like grains, the number of which decreases with increasing solution concentration. Using CuO0.1M prevents the formation of nano petals. Since creation starts at 0.2M, CuO0.2M achieves the maximum nano petal coverage on micro grains.

This distinctive "nano-petals on microgranuales" type CuO form is an interesting hierarchical structure as it provides a greater surface area to volume ratio. The first step involves the formation of nano-petals atop microgranuales, which are believed to have been quickly deposited because of the fast reaction time (5 minutes). Although numerous odd (micro)

morphologies have been documented for CuO in the literature, this is the sole known form at this time. When it comes to morphologies, the deposition process and preparative conditions usually play a big role. There are various documented processes for CuO, including electrodeposition on copper substrate, sol-gel, surface oxidation of Cu-foil, and hydrothermal methods. The former method yields an aggregate that looks like cauliflower, while the latter produces elongated grains, nanoflakes, angular-shaped crystallites, and nanorods. The morphology may be customized by using various substrates. A complex nanoscale morphology with aggregation of densely packed nanorods with aspect ratio is seen in thin films of CuO produced by the hydrothermal technique from copper acetate precursors. Contrarily, nanoscale structures using 2-piperidine methanol necessitated a reaction period of 24 hours. The complex nanoscale morphology, however, shows that this stated formula does not accomplish precise control over growth.

Outperforming the previous research, our results demonstrate the distinct impact of hierarchical nano petals on microgranule morphology. The management of the preparative parameters is better since the response time is much shorter (5 minutes) than the indicated 24 hours.

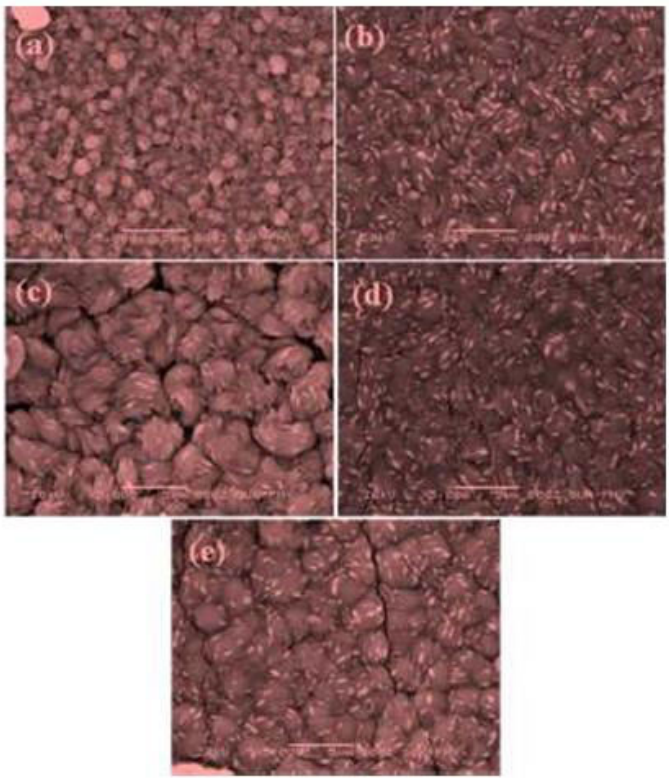

Fig 4: Scanning Electron Micrographs of the (a) $CuO_{0.1M}$(b) $CuO_{0.2M}$(c) $CuO_{0.3M}$(d) $CuO_{0.4M}$ (e) $CuO_{0.5M}$ samples at X5000 magnifications.

Electrochemical Impedance Spectroscopic Measurement:

According to the conventional three-electrode arrangement, graphite was used as the counter electrode and a saturated calomel electrode (SCE) as the reference electrode for the

electrochemical investigations in 0.1M [HPMIM][Cl] IL. An American-made CH Instrument CHI-400A scanning potentiostat was used. The charge-discharge electrochemical impedance spectroscopy (EIS) experiments were carried out in a three-electrode cell with a platinum counter electrode using SCE as a reference using a Wonatech WMPG 1000-Potentiostat-Galvanostat. Electrochemical impedance spectroscopy (EIS) studies are useful for learning more about equivalent series resistance and resistance to redox processes. In this study, impedance was evaluated using a frequency range of 0.1 to 1 x 10^1 Hz.

Figure 5 shows the Nyquist plots generated at open circuit potential after the placement of all samples in a three-electrode cell setup in an aqueous solution of 0.1 M [HPMIM][Cl] IL. From CuO0.1M to CuO0.2M samples, the intercept of the plot with the real impedance (Z) axis decreases, and from CuO0.3M to CuO0.5M samples, it increases again. Actually, the intercept represents the sum of the three variables: the electrolyte (Re), the electrode active material (Ra), and the combined uncompensated electrical resistance (Rl) [11, 12]. With a low resistance of 7.73 Ω in the high frequency band, the sample outperforms other samples in terms of conductivity. There has been a dearth of scholarly publication coverage of EIS measurements. But our results were only corroborated by a small number of reports.

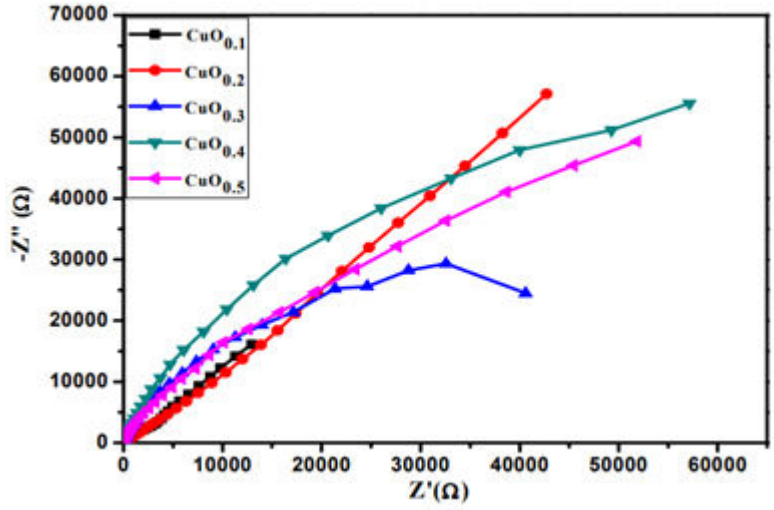

.

Fig. 5: Nyquist plot for all the samples in 0.1 M [HPMIM][Cl] IL electrolyte

AFM analysis

Atomic force microscopy (AFM) was used to analyze the material's morphology [10]. In Table 2, you can see the collected data, which includes RMS, Rs, and Pav, which stand for particle size and root mean square. There seems to be a relationship between particle size and thickness, because Pav showed a reduction with increasing thickness. At a 300 nm thickness, RMS also showed a drop from 9.18 nm to 4.29 nm, which was similar to the pattern shown in Rs, which also reduced from 9.30 nm to 4.71 nm. Table 2 shows that values for surface roughness and particle size decrease with increasing thickness. This is consistent with the previous results.

ISSN PRINT 2319 1775 Online 2320 7876
 UGC CARE Listed (Group -I) Journal Volume 12, Iss 01, 2023

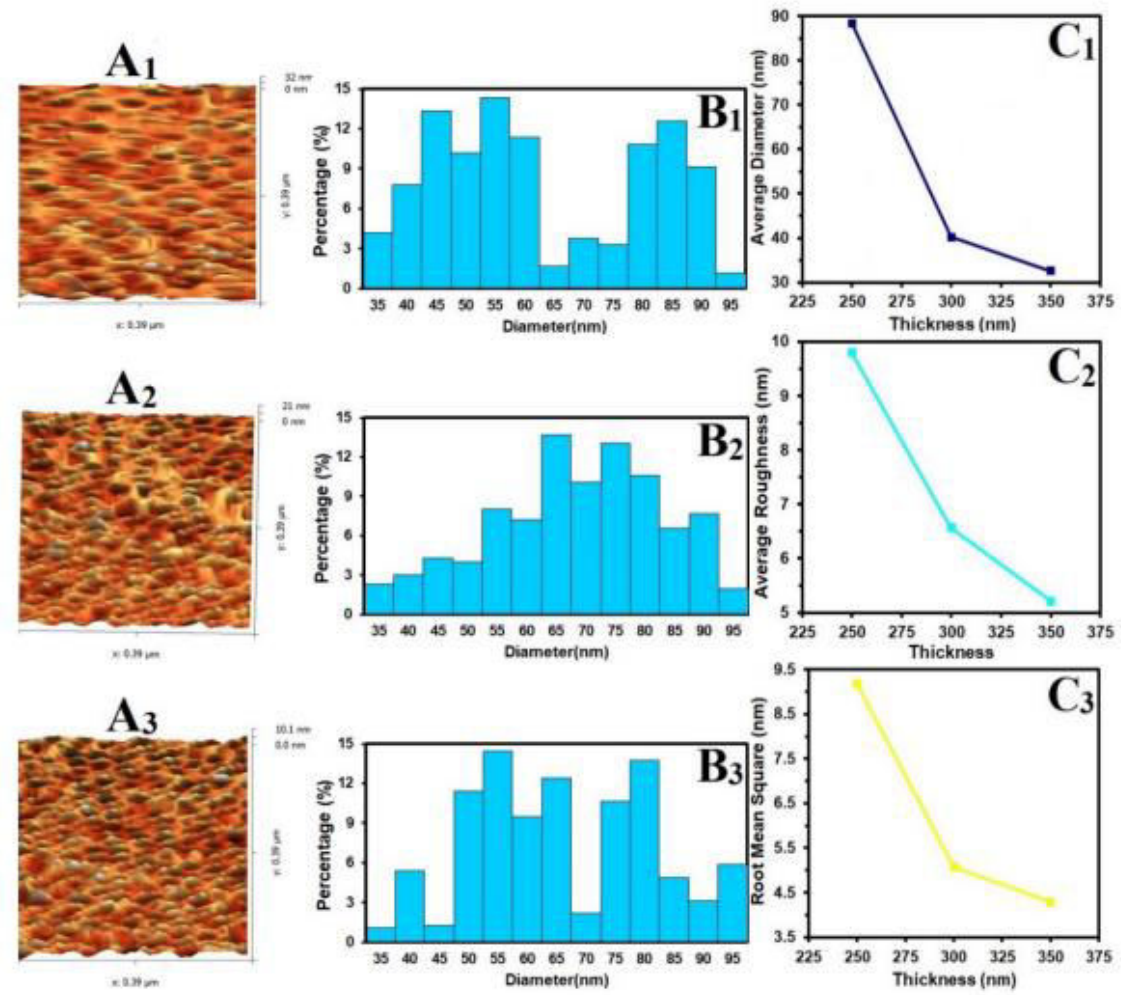

Fig. 6. AFM information of CuO films.

Table 2. AFM parameters of (CuO) thin film with different thicknesses.

Thickness (nm)	P_{av} nm	R_s (nm)	RMS (nm)
250	88.4	9.30	9.18
300	40.2	6.07	5.08
350	32.6	4.71	4.29

CONCLUSION

The shape, optical characteristics, and polycrystalline nature of CuO thin films produced by (RF) magnetron sputtering were investigated in our work. Based on the XRD data, we determined that the average grain size is 10.78, 11.36, and 11.84 nm for thicknesses of 250,

300, and 350 nm, respectively. From 250 to 350 nm in thickness, the AFM roughness dropped from 9.18 to 4.29 nm. Grain sizes vary from 26.67 to 44.9 nm, as seen in scanning electron microscopy photographs, which progressively increase with increasing thickness. It was shown that as thickness increases, transmittance decreases and absorption increases for the given wavelength range.

REFERENCES

1. Şahin, Mustafa & Blaabjerg, F. &Sangwongwanich, Ariya. (2022). A Comprehensive Review on Supercapacitor Applications and Developments. Energies. 15. 674. 10.3390/en15030674.

2. Czagany, Mate &Hompoth, Szabolcs &Keshri, Anup & Pandit, Niranjan & Galambos, Imre & Gácsi, Zoltán & Baumli, P.. (2024). Supercapacitors: An Efficient Way for Energy Storage Application. Materials. 17. 702. 10.3390/ma17030702.

3. Deep, Aman & Gupta, Anish & Singh, Shamsher & Khatoon, Nahida &gupta, Gopal. (2024). Overview of Supercapacitors: A Comprehensive Review. 10.20944/preprints202405.1509.v1.

4. Schneuwly, Adrian & Gallay, Roland. (2020). Properties and Applications of Supercapacitors From the State-of-the-art to Future Trends.

5. Kosnan, Muhammad & Azam, Mohd Asyadi& Takasaki, Akito. (2023). Applications of Green Supercapacitors in Transportation Systems. 10.1039/BK9781837672479-00352.

6. Pandolfo AG, Hollenkamp AF (2016) Carbon properties and their role in supercapacitors. J Power Sources 157:11–27. doi:10.1016/j. jpowsour.2006.02.065

7. Senthilkumar V, Kim YS, Chandrasekaran S et al (2015) Comparative supercapacitance performance of CuO nanostructures for energy storage device applications. RSC Adv 5:20545–20553. doi:10.1039/C5RA00035A

8. Gund GS, Dubal DP, Jambure SB et al (2013) Temperature influence on morphological progress of Ni(OH)2 thin films and its subsequent effect on electrochemical supercapacitive properties. J Mater Chem A 1:4793–4803. doi:10.1039/c3ta00024a

9. Shinde SK, Dubal DP, Ghodake GS et al (2014) Nanoflower-like CuO/Cu(OH)2 hybrid thin films: synthesis and electrochemical supercapacitive properties. J Electroanal Chem 732:80–85. doi:10.1016/j.jelechem.2014.09.004

10. Pell WG, Conway BE (2011) Analysis of power limitations at porous supercapacitor electrodes under cyclic voltammetry modulation and dc charge. J Power Sources 96:57–67. doi:10.1016/S0378- 7753(00)00682-0

11. Dubal DP, Gund GS, Lokhande CD, Holze R (2013) Decoration of sponge-like Ni (OH) 2 nanoparticles onto MWCNTs using an easily manipulated chemical protocol for supercapacitors. ACS Appl Mater Interfaces. doi:10.1021/am3026486

12. Jagadale AD, Kumbhar VS, Dhawale DS, Lokhande CD (2013) Potentiodynamically deposited nickel oxide (NiO) nanoflakes for pseudocapacitors. J Electroanal Chem 704:90–95. doi:10.1016/j. jelechem.2013.06.020

13. Jagadale AD, Kumbhar VS, Dhawale DS, Lokhande CD (2013) Performance evaluation of symmetric supercapacitor based on cobalt hydroxide [Co(OH)2] thin film electrodes. Electrochim Acta 98:32–38. doi:10.1016/j.electacta.2013.02.094

14. QT Q, Wang B, Yang LC et al (2018) Study on electrochemical performance of activated carbon in aqueous Li2SO4, Na2SO4 and K2SO4 electrolytes. ElectrochemCommun 10:1652–1655. doi:10.1016/j.elecom.2008.08.020

15. Wen ZB, QT Q, Gao Q et al (2019) An activated carbon with high capacitance from carbonization of a resorcinol-formaldehyde resin. ElectrochemCommun 11:715–718. doi:10.1016/j. elecom.2009.01.015